4.2.2. Solution of the reactor model

The set of algebraic equations resulting from the discretization of a PDE is first reduced to the standard form shown in equation 4–6. This is accomplished by solving the linear equations of the boundary conditions for the values of y at the boundary. The boundary values are then substituted into the equations of the discretized PDE giving a total of NR·NZ equations of the form:

$$\mathbf{Dy} + \mathbf{g} + \mathbf{r} = 0 \qquad (4\text{–}6)$$

where **y** is a vector of the dependent variable at the interior grid points, D is a matrix containing combinations of elements from the collocation matrices and the model parameters, **g** is a vector dependent on the input values of y and **r** is a vector of reaction rates at the grid points. If the kinetics are non–linear equation 4–6 becomes non–linear. The matrix D is constant if the model parameters are independent of conversion. The necessary steps of algebraic manipulations in order to obtain equation 4–6 are given in detail by Windes (Windes, 1986).

If there are more than one PDE, more equation sets are obtained, and the sets may be coupled through the kinetics. The sets can be combined to give one set of the form shown in equation 4–6, where **y** now is composed of the elements $\mathbf{y}_1,\ldots,\mathbf{y}_i,\ldots,\mathbf{y}_{NR\cdot NZ}$. The element $\mathbf{y}_i$ is a vector of all the dependent variables at a grid point.

The equation system 4–6 can be solved by the Newton–Raphson method shown in equation 4–7, or the faster successive substitution method (Finlayson, 1974) shown in equation 4–8. The Newton–Raphson method should be tried if the successive substitution method fails to converge. It can be advantageous not to lump all equation systems into one big system, but instead lump into a few smaller systems and solve the systems in a nested fashion. This can give the solution procedure better convergence properties. The principles for solving the two nested sets of equations $\{\mathbf{f}(\mathbf{y}_1,\mathbf{y}_2)=0;\ \mathbf{g}(\mathbf{y}_1,\mathbf{y}_2)=0\}$ are to solve $\mathbf{g}(\mathbf{y}_1,\mathbf{y}_2)=0$ with respect to $\mathbf{y}_2$, using a constant value for $\mathbf{y}_1$. This is done after each iteration of $\mathbf{f}(\mathbf{y}_1,\mathbf{y}_2)=0$. The value of $\mathbf{y}_1$ used in **g** is obtained from the iteration of **f**, and **f** is only solved with respect to $\mathbf{y}_1$. The value

of y_2 used in **f** is obtained from the solution of **g** at each iteration step of **f**.

For the fluid phase model it was found that lumping of all the mass balances into one set of equations and solving the heat balance and the lumped mass balances as nested sets was the best choice to ensure convergence. In the notation used above the nesting is defined as:
{heat_balance(temperatures, concentrations);
mass_balances(temperatures,concentrations)}

The solid phase model equations, if applied, are solved at each fluid phase grid point at each iteration of the fluid phase equations. From the solution of the solid phase equations the mean pellet reaction rates are calculated using the integration formula and the quadrature weights given by Villadsen and Stewart (Villadsen and Stewart, 1967). The calculated mean rates are passed on to the rate vector, **r**, of the fluid phase equations.

The program has the option of choosing between Newton–Raphson and the successive substitution method in solving the equation sets. The iteration formulaes used to solve equation 4–6 are given by equation 4–7 and 4–8.

Iteration formulaes:

Newton–Raphson

$$\mathbf{J}\mathbf{y}^{k+1} = (\partial \mathbf{r}/\partial \mathbf{y})\mathbf{y}^{k} - (\mathbf{g} + \mathbf{r}(\mathbf{y}^{k})) \qquad (4\text{–}7)$$

where $\mathbf{J} = \mathbf{D} + \partial \mathbf{r}/\partial \mathbf{y}$

Successive substitution

$$\mathbf{D}\mathbf{y}^{k+1} = -(\mathbf{g} + \mathbf{r}(\mathbf{y}^{k})) \qquad (4\text{–}8)$$

4.3. PROGRAM STRUCTURE

This chapter outlines the main structures of the computer implementation for the reactor model and it's solution as described in the previous chapters. The various data needed for definition of the model, and for definition of data areas for storing parameters, grid definitions, matrices used for discretization and results from the model solution are grouped together in data structures. This is accomplished by the use of the structure definition in the C language. Furthermore, there are structures for partitioning of the dependent variables into equation sets or partitioning between different phases. An equation set is defined by equation 4–6. The equation sets are stored in an array and are solved in a nested fashion as described in chapter 4.2. The definitions of the main structures and their connections are shown in Figure 4–1.

The main program structure is shown in Figure 4–2. In addition to the mathematical subroutines, the program contains subroutines for managing the structures. These are subroutines for initializing the structures and for updating with new data. Dynamic memory allocation is used both for initializing structure data areas and for resizing at update. The grid structure data space is initialized to zeros at allocation.

All matrices are stored in memory locations corresponding to consecutive columns, like it is done in FORTRAN. Thus, standard FORTRAN routines could be used for matrix manipulations. Solution of the iteration equations 4–7 and 4–8 is performed by LU decomposition using gaussian elimination with partial pivoting, followed by backsubstitution.

Estimation of parameters from experimental data was accomplished by interfacing the model program to a parameter estimation package. The MODFIT program was used for this purpose (Hertzberg, 1970). It uses the SIMPLEX method (Nelder and Mead, 1965) to locate the optimum of the object function. Optionally a second order surface can be fitted to the output at the obtained optimum to locate a more exact optimum and to calculate parameter statistics. A least square criterion was choosen as the object function.

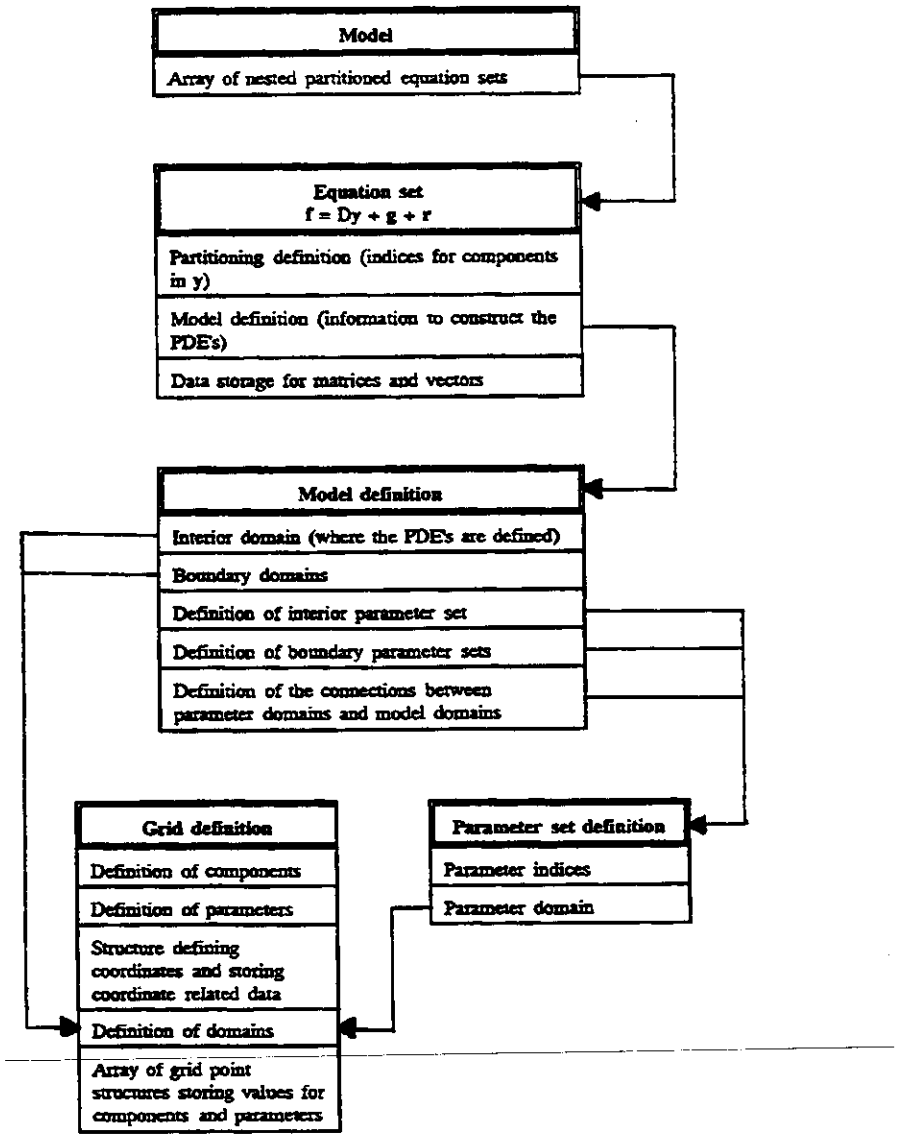

Figure 4–1. Arrangement of main data structures.

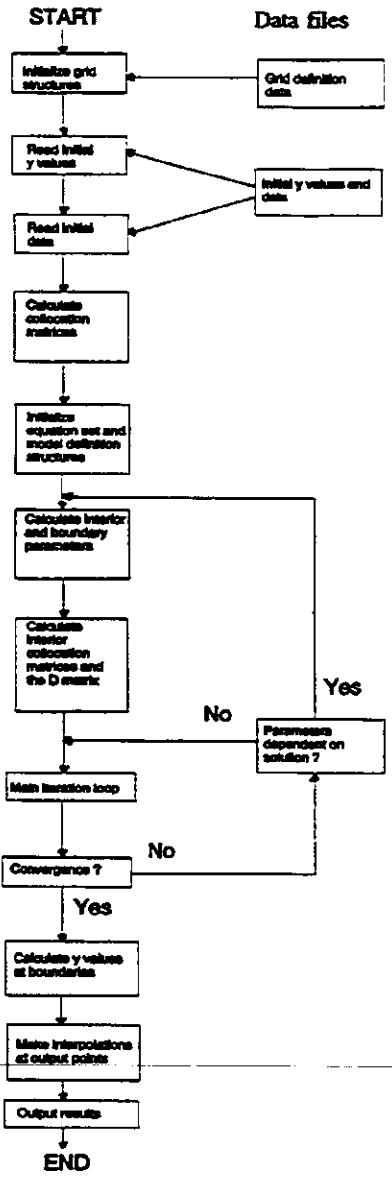

Figure 4–2. The program structure.

4.4. PARAMETERS

The mass dispersion coefficients and the effective axial conductivity are relatively unimportant parameters in the sense that the model output is rather insensitive to variations in their values at normal steady state conditions. These parameters were therefore assumed to have constant values, independent of radial position. The values used were obtained from available correlations, and the correlations used were the ones recommended by Vortmeyer and Haidegger (Vortmeyer and Haidegger, 1991) They are listed in equations 4-9 to 4-11. The static contribution to the effective thermal conductivity of the bed, λ^0_e, was estimated from the relation shown in equation 2-17.

Further assumptions made in the modeling were that the superficial velocity and the physical properties of the fluid phase are independent of conversion. For the Fischer-Tropsch synthesis there is actually a decrease in velocity and an increase in fluid density with increasing conversion, but the dilution with nitrogen used in the experiments will diminish these effects. Both velocity and fluid properties were calculated at inlet conditions. Simulation input data for the three experiments are shown in Table 4-2.

$$\frac{1}{Pe_{mz}} = \frac{1-\sqrt{1-\varepsilon_0}}{Re_p Sc} + \frac{1}{2} \qquad (4\text{-}9)$$

$$\frac{1}{Pe_{mr}} = \frac{1-\sqrt{1-\varepsilon_0}}{Re_p Sc} + \frac{1}{8.8\left[2-\left(1-\frac{2d_p}{d_t}\right)^2\right]} \qquad (4\text{-}10)$$

$$\frac{1}{Pe_{hz}} = \frac{\lambda^0_g/\lambda_g}{Re_p Pr} + 0.7 \qquad (4\text{-}11)$$

Reactor dimensions and catalyst properties are shown in Table 4–1. Details on reactor design are given in chapter 3.3 and on the catalyst in Appendix I.

Table 4–1. Reactor and catalyst data.

L (m)	1.5
R (m)	12.5×10^{-3}
R_O (m)	17.5×10^{-3}
ρ_b (kg/m^3)	0.89×10^3
ρ_p (kg/m^3)	1.59×10^3
ε_0	0.44
ε_p	0.485
d_p (m)	3.3×10^{-3}
C_{ps} (J/(kg K))	965
λ_p (W/(m K))	0.4
α_c (W/(m^2 K))	430
λ_w (W/(m K))	18.0

The values of the solid phase heat capacity, C_{ps}, and the effective conductivity of the catalyst particles, λ_p, were not known for the specific catalyst used in this study. Thus the values reported in Table 4–1 had to be estimated from available literature data. The accuracy of this approach may be difficult to judge, but these parameters are relatively unimportant in steady state simulations models for the same reason as for the mass dispersion and axial conductivity.

Since little is known about composition and structure of the cobalt–oxide phase, the heat capacity is taken to be that of amorphous silica which constitutes about 50 % of the catalyst. The value is taken from Perry (Perry, 1984) at 500 K.

The thermal conductivity of porous pellets depends on the conductivities of the solid and fluid phases, the pore structure and the contact area between the particles making up the pellet. This parameter is therefore a complex function of a number of factors and should preferentially be determined by measurements on the actual catalyst. Harriott (Harriott, 1975) has presented some relations for estimation of the pellet conductivity based on particle models, but these relations are dependent on parameters which are often unknown. A value of about 0.4 W/m K has been reported for silica–alumina cracking catalysts with mean pore size less than 50 Å and a relatively narrow distribution (Harriott, 1975). Since silica is the main constituent of the catalyst used in this study and the pore size distribution is narrow with a relatively small mean pore size (Appendix I), a value of 0.4 W/m K is used for the pellet conductivity.

The parameter λ_w in Table 4–1 is the thermal conductivity of the stainless steel reactor wall and α_c is the heat transfer coefficient at the coolant side of the reactor wall. The value of the latter was estimated from data on Dowtherm G heat transfer oil given by the supplier (Dowtherm Organic Heat Transfer Fluids, The Dow Chemical Company) and available correlations on heat transfer coefficients at the annulus between concentric tubes (VDI–Wärmeatlas, 1984, p. Gd2). The value reported in Table 4–1 was calculated at 500 K for the reactor dimensions and oil circulation capacity given in chapter 3.3.

Table 4–2. Summary of model input and fluid data used for simulations and parameter estimation.

Run no.	1	2	3
T_c (K)	497	499	499
Inlet conditions			
T_0 (K)	498	503	500
P^0_t (MPa)	1.0	1.0	1.0
P_{N_2} (MPa)	0.77	0.82	0.70
v_0 (m/s) [1]	0.16	0.15	0.15
C_{0,N_2} (mol/m^3) [1]	186.0	196.1	168.4
$C_{0,CO}$ (mol/m^3) [1]	17.4	13.5	22.6
C_{0,H_2} (mol/m^3) [1]	38.2	29.6	49.6
Physical properties of the gas mixture at inlet conditions			
ρ_g (kg/m^3) [1]	5.77	5.93	5.45
C_{pg} (J/(kg K)) [2]	1333	1295	1398
μ_g (N s/m^2) [2,4]	2.56×10^{-5}	2.58×10^{-5}	2.56×10^{-5}
λ_g (W/(m K)) [3,5]	0.05972	0.05526	0.06701
Dimensionless groups related to inlet conditions			
Re_p	119	113	105
Pr	0.57	0.60	0.53
Carbon number distribution parameters (weighted average values at reactor outlet)			
α	0.69	0.64	0.68
γ	0.88	0.86	0.93

[1] Estimated from the ideal gas law at inlet temperature and pressure.

[2] Data for the individual components were estimated from relations given by Lydersen (Lydersen, 1979, Appendix 2).

[3] Data for the individual components were estimated from relations given by Reid et. al. (Reid et al., 1987, Table 10–3).

[4] Viscosity of mixture was estimated by Wilke's method (Reid et al., 1987, p. 407).

[5] Thermal conductivity of mixture was estimated by Mason and Saxena's method (Reid et al., 1987, p. 531).

Values for the molecular diffusivities of the gases are needed for the estimation of effective diffusivities in the bed. These values are given in Table 4–3. They are binary diffusion coefficients calculated from the Chapman–Enskog relation (Reid et al., 1987, p. 581) with N_2 as the second component. This simplification was done because the feed gas was highly diluted with nitrogen in the experiments.

Table 4–3. Gas phase diffusion coefficients, T=500 K, P=1.0 MPa

Component	Molecular diffusivity D_m (m^2/s)
CO	4.96×10^{-6}
H_2	1.81×10^{-5}
CH_4	5.44×10^{-6}

5. RESULTS AND DISCUSSION

5.1. INTRODUCTION

The first object of the experimental work was to make an evaluation of the performance of the reactor and to see if the plant, analysis system and control system performed up to expectations. When this was established, a search for an area of useful steady state operating conditions was performed. Initially it was determined to restrict the range of operating conditions to an area where substantial amounts of high molecular weight products are not likely to be formed. This was done because on–line analysis of high molecular weight products on a gas chromatograph was considered problematic as it can be expected that such products are not in the gas phase under reaction conditions. This may give inaccurate mass balances as well as wax condensation and possibly plugging of the small diameter tubes in the analysis system. It was therefore decided to restrict the lowest operating temperature to ca. 483 K and the lowest H_2/CO ratio to ca. 2.

All experiments were carried out at 1.0 MPa total pressure with nitrogen as diluent. The temperature at the reactor inlet was kept approximately equal to the oil temperature. The pressure and space velocity of synthesis gas were varied while the gas flow of nitrogen was kept in the high range of the flow–controller in order to minimize heat and mass transfer limitations. The initial tests showed that the reactor was very sensitive to variations in temperature and partial pressure of synthesis gas with this highly exothermic reaction, and that only a narrow range of temperatures could be used for steady state experiments when other operating conditions were fixed. Below this range, virtually no reaction occured, and above the range the reactor became unstable resulting in a thermal runaway of several hundred degrees. The progression of such a runaway is shown in Appendix II. Due to these restrictions, temperature could not be chosen freely but was dependent on the other variables.

At partial pressures of synthesis gas belov ca. 0.3 MPa the useful steady state operating temperature was about 500 K and relatively independent of the pressure. At higher partial pressures instability problems became more severe, and possibly useful operating temperatures

seemed to be much lower than 500 K which could lead to formation of mainly wax products.

During the first hours on stream in each run the catalyst showed an apparent rapid declining activity which after a time levelled out as indicated by the rate of decline of the temperature differences across the reactor bed. Because of this higher initial activity the start temperature had to be set lower than the steady state temperature, and temperature was gradually increased until steady state was obtained. But even at steady state there was a slow decline in catalyst activity as shown in chapter 5.2. The higher initial activity was completely restored when performing a new run after shutdown of the previous run using the same catalyst load.

Three steady state experiments were performed. The object of these experiments was to provide data for use in model evaluation and parameter estimation. During each experimental run a complete axial concentration and selectivity profile was recorded by taking a FID and a TCD analysis at each of the ten positions in the reactor as well as an inlet gas analysis. Temperature profiles were recorded at frequent intervals during experiments.

The main object of the reactor modeling was to evaluate the heat transfer characteristics of the bed under reactive conditions, and to estimate heat transfer parameters from experimental data. The kinetic study was therefore mainly concerned with reactions of importance for heat generation in the bed. For a Fischer–Tropsch catalyst with low shift activity these are the rate of CO consumption and the rate of methane formation.

The experimental investigations were performed on a catalyst with no prior knowledge of the kinetic and selectivity parameters exept for the general conclusions which can be drawn from literature data. Before any model evaluations could be done, a kinetic model had to be established and kinetic parameters had to be estimated. This was done using data from the three steady state experiments although determination of kinetic data from a non–isothermal fixed bed reactor under a restricted set of operating conditions is not completely satisfactory.

The kinetic parameters thus obtained were then used in models for further evaluation of the heat transfer characteristics of the bed. The models were of the pseudo–homogeneous type, both with constant and radial dependent parameters and velocity.

5.2. EXPERIMENTAL RESULTS

This chapter summarizes the results from the three experiments at steady state conditions. The runs were performed in sequence using the same catalyst load. During start up of run 3 a thermal runaway occured causing a permanent deactivation of the catalyst. The catalyst showed about the same activitiy in run 1 and 2, but the activity in run 3 was somewhat lower. Experimental conditions and conversion and selectivity at reactor outlet are shown in Table 5–1. The hydrocarbon product mainly consisted of n–alkanes with smaller amounts of alkenes and isomers. Oxygenates were not detected. Details on product analysis and selectivity calculations are given in Appendix II.

Table 5–1. Effect of experimental conditions on catalyst activity and selectivity.

Run no.	1	2	3
Wall temperature (K)	497	499	499
Inlet conditions			
Temperature (K)	498	503	500
Total pressure (MPa)	1.0	1.0	1.0
P_{H_2+CO} (MPa)	0.23	0.18	0.30
H_2/CO molar ratio	2.2	2.2	2.2
GHSV (Nl_{H_2+CO}/kg catalyst · h)	540	400	670
Outlet conversion and selectivities			
CO conversion (%)	34.4	48.5	24.5
Carbon selectivities (%)			
CH_4	16.0	18.4	14.5
C_2–C_4	29.7	34.7	29.5
C_{5+}	47.8	42.9	44.9
CO_2	6.6	4.1	11.1
Carbon recovery (%)	96.1	90.1	90.8

During each experimental run a complete axial composition profile was recorded exept for run 1 where analyses at z = 1.2 m and 1.35 m are missing due to a plugging of the sampling tubes caused by catalyst dust. It took about 2 hours to complete an analysis in one reactor position before moving to the next position. As a consequence the analysis points in the profiles were recorded at different catalyst activity since the catalyst deactivated slowly with time. This means that the recorded axial composition profiles are not "true" axial profiles, but are somewhat distorted by the time dependence. This time dependence also caused slight errors in carbon balance calculations since the analyses on the TCD and the FID had to be taken consecutively. The FID analysis was taken first and the TCD more than an hour later. But the carbon balances were normally within 90 to 100 % except near the inlet where conversion was low.

In run 1 the axial composition profile was recorded sequentially from inlet to outlet. The results are shown in Figure 5–1 where increasing distance from inlet also means increasing time. To get an idea of the effect of time, two consecutive profiles were recorded in the two other runs taking analyses sequentially from inlet to outlet at every other axial point within each profile. The results are shown in Figures 5–2 and 5–3. Details on sampling order for each profile and composition data at each sampling point are given in Appendix II for the three runs.

The data of Appendix II also includes the Schulz–Flory parameter, α, obtained from a plot of $\ln(X_n)$ versus n for the C_3–C_{10} fraction at the various axial positions. The values of α thus obtained are weighted average values depending on the local values at all previous reactor positions. If the hydrocarbon distribution follows Schulz–Flory in each point in the reactor then the average distribution detected at reactor outlet will also approximately follow the Schulz–Flory distribution with a weighted average value of α. Deviations become pronounced only for hydrocarbons with more than ten carbon atoms (Lox and Froment, 1993a). Schulz–Flory plots at reactor outlet for the three runs are shown in Appendix II for the C_1–C_{20} fraction. These plots show that the C_3–C_{10} fraction closely follows Schulz–Flory and that the C_1 fraction is higher and the C_2 fraction lower than expected. These deviations for C_1 and C_2 are commonly observed on cobalt and iron Fischer–Tropsch catalysts.

The effect of deactivation is shown in the differences of the CO conversion profiles in Figures 5–2 and 5–3 and in the decreasing reactor temperatures with increasing time shown in Figure 5–5. Because of the correlation between temperature and catalyst activity this decrease in temperature will be partially responsible for the decrease in conversion with increasing time on stream and may affect selectivities too. Both the rapid initial deactivation and the long term more slow deactivation have been described in the literature, but the underlying causes of these observations seem not fully understood. Formation of inactive carbonacous deposits, sintering and changes in the catalyst composition with time have been proposed as explanations of the observed deactivation, e.g. (Bukur et al., 1990). It is known that unpromoted cobalt catalysts like the one used in this study, show poorer stabilty than promoted catalysts (Winthers et al., 1990; Varma et al., 1985).

Liquid accumulation in the catalyst pores is known to impose intraparticle mass transfer restrictions on reactants and products, thus lowering the observed rate of CO conversion (Zimmerman et al., 1989; Post et al., 1989; Iglesia et al., 1993) and may also affect selectivity (Iglesia et al., 1993). Bukur et al. (Bukur et al., 1990) attributed the rapid loss of activity during the first 50 hours on stream in the fixed bed reactor to such an accumulation. It is, however, not likely that the initial rapid loss of activity observed in this study can be attributed to increased mass transfer limitations caused by liquid accumulation in the pores. Concerning the low selectivity to high molecular hydrocarbon products obtained, it can be expected that it would have taken a quite a long time to fill up the pores with liquid. With values of the chain growth probability below 0.7 as shown in Figure 5–4, it can be estimated from the simulations of Huff and Satterfield (Huff and Satterfield, 1985) that the time to fill up the first pore must be several hundred hours or more. But the long term deactivation observed to persist throughout the duration of each run may at least partially be caused by an increasing pore fraction being filled with liquid.

While the CO_2 selectivity generally is below 5 % and fairly independent on axial position and time, some exeptions are noted in Figures 5–2 and 5–3. There seem to be a noticeable increase in CO_2 selectivity towards the reactor outlet at longer times on stream. These exeptions are denoted at z = 1.35 m in run 2 and 3 while an analysis is missing at this point in run 1. A less pronounced effect is also denoted at the outlet in run 3. Furthermore, an

increase in conversion is observed at the same points. A detailed analysis of the axial concentration profiles showed that the yield of the C_{5+} fraction as well as the carbon number distribution of this fraction (Figure 5–4) are not affected by the anomalies at these points. So concerning the production of C_{5+} hydrocarbons, the catalyst operates normally although their selectivity is lower because of higher CO conversion. The increase in conversion leads to formation of methane and ethane with about the same selectivity as normal, but the rest of the product is just CO_2.

An explanation of these irregularities could be structural or compositional changes in the oxidic phase of the catalyst during an experimental run, turning inactive points into active ones. The catalyst contained substantial amounts of unreduced cobalt oxide (Appendix I) and production of significant amounts of CO_2 is reported to occur on poorly–reduced cobalt catalysts (Reuel and Bartholomew, 1984). Furthermore shifts in selectivity towards lighter hydrocarbons (Winthers et al., 1990; Varma et al., 1985) are reported at longer times on stream for cobalt catalysts. But explanations involving changes in the catalyst performance is questionable taking into account that the conversion and selectivity curves represent integral values where the conversion and selectivities at the outlet are weighted averages of the values throughout the whole reactor. Drastic changes must have occured with the catalyst near the outlet within a short period of time towards the end of the run if such an explanation is correct. Another explanation could be that a local hot spot had developed in the bed at the entrance of the sampling tube at $z = 1.35$ m, or catalyst dust could have entered the sampling tube and created a hot spot inside the tube. There were weak indications of irregularities in the temperature profile at this point in the reactor because of a peak in the wall temperature of a few degrees at this point during all the runs. But the thermocouples at the other two radial positions showed no such deviations. A local hot spot possibly originating from a catalyst particle of higher activity or maldistribution of the flow pattern around the entrance of the sampling tube could cause an increased conversion located to this area giving rise to analysis data not representative for the bulk gas phase. Conversion at higher temperatures would be expected to give mainly light hydrocarbons and CO_2 from the shift reaction (Huff and Kobylinski, 1991; Gottschalk et al., 1988). But the question of the higher conversion and CO_2 selectivity at $z = 1.5$ m observed in run 3 remains unanswered by this explanation. It is thus not possible to give a satisfactory explanation of the observed deviations. But the

observations are real in the sense that there are no indications of analytical errors.

The rate of formation of CO_2 by the shift reaction on cobalt catalysts increases with increasing partial pressure of water and is inhibited by CO at least at higher partial pressures (Grenoble and Estadt, 1981; Huff and Kobylinski, 1991). The selectivity to CO_2 caused by the shift reaction should thus increase with increasing conversion (Huff and Kobylinski, 1991) and therefore, an increase in CO_2 selectivity should be observed with increasing distance from the inlet. Under normal catalyst operation the selectivity is, however, rather constant. The selectivity value of about 5% observed in run 1 and 2 is also somewhat higher than can be expected on a Co on SiO_2 catalyst (Varma et al., 1985; Withers et al., 1990). It is therefore not unlikely that the CO_2 produced when the catalyst operates with a low CO_2 selectivity comes from other reactions than the shift reaction. This could be the Boudouard reaction (equation 2–44). The exceptionally high CO_2 selectivity observed is, however, most likely attributed to increased shift activity caused by either structural changes in the catalyst, a local hot spot or possibly some other unknown effect.

Apart from the deviations discussed above the selectivities shown in Figures 5–1 to 5–3 and the chain growth probabilities shown in Figure 5–4 reveal only small variations in their values with reactor position and time on stream. This was expected because the variations in temperature were small, and the H_2/CO ratio of the feed gas was kept near the usage ratio. It follows from chapter 2.3.4. that the main influence on selectivity comes from temperature and the H_2/CO ratio. Generally there is a slight decrease in methane selectivity and a correspondingly increase in the selectivity of higher molecular weight hydrocarbons with increasing distance from the inlet, and also with increasing time on stream for run 2 as shown in Figure 5–2. These variations may at least partially be explained by the variations of temperature with axial position and time on stream.

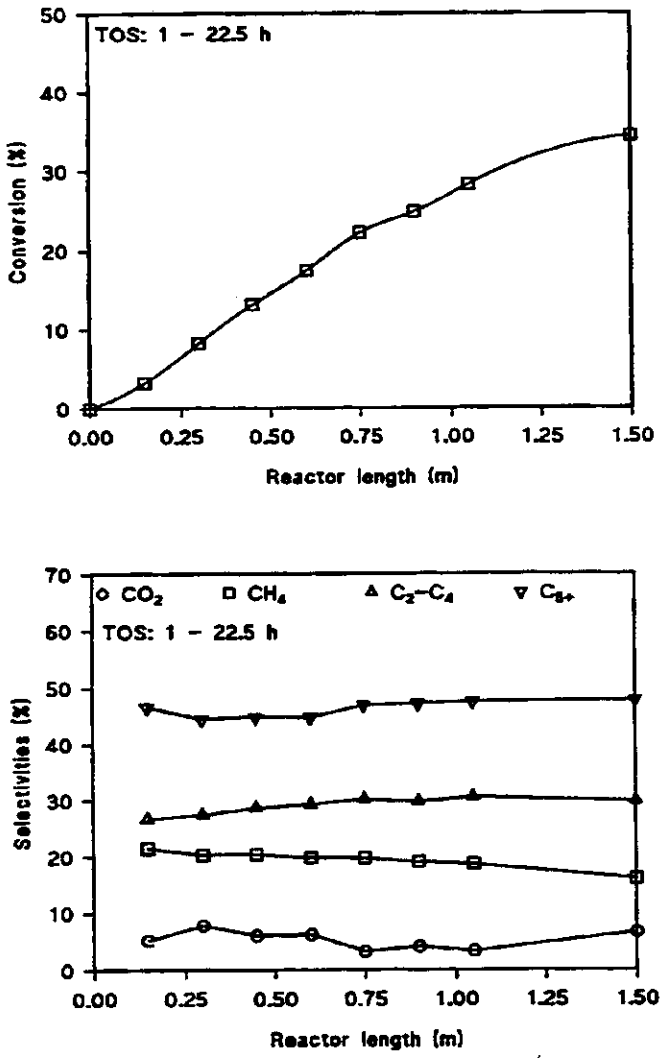

Figure 5–1. CO conversion and product selectivities dependent on axial reactor position and time on stream for run 1. The data points were recorded in sequence from inlet to outlet within the specified time interval. Experimental conditions are given in table 5–1.

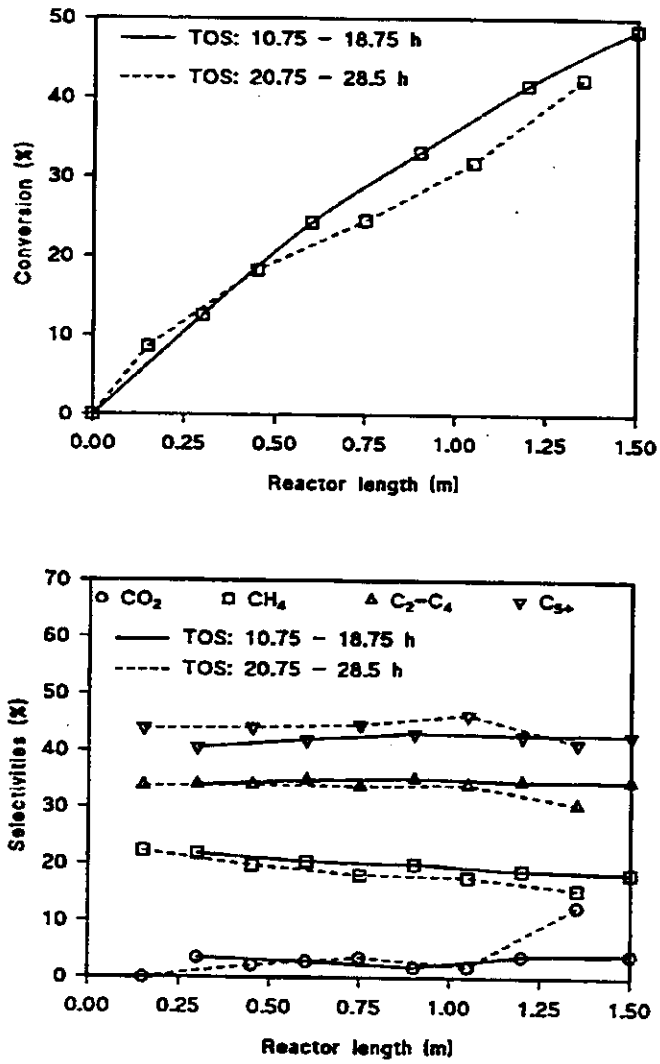

Figure 5–2. CO conversion and product selectivities dependent on axial reactor position and time on stream for run 2. The data points were recorded in sequence from inlet to outlet within the specified time intervals. Experimental conditions are given in table 5–1.

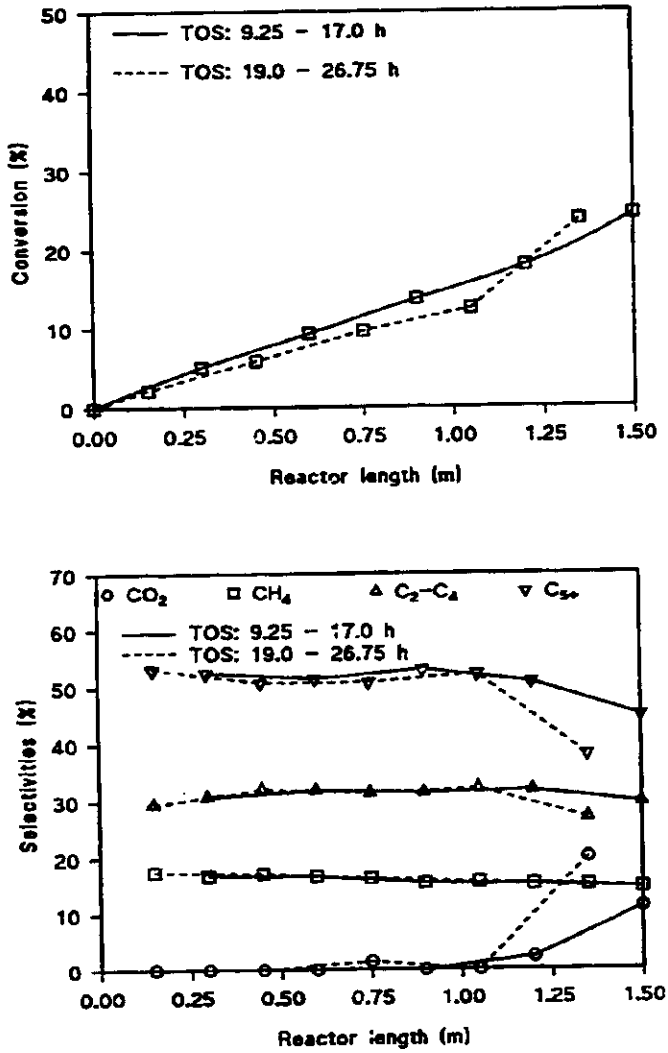

Figure 5–3. CO conversion and product selectivities dependent on axial reactor position and time on stream for run 3. The data points were recorded in sequence from inlet to outlet within the specified time intervals. Experimental conditions are given in table 5–1.

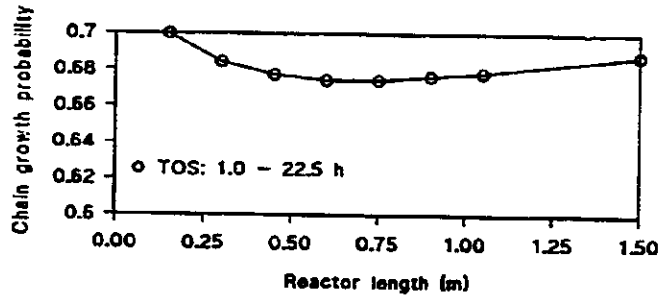

Run 1

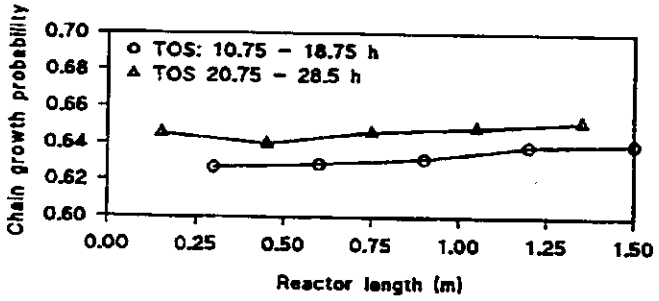

Run 2

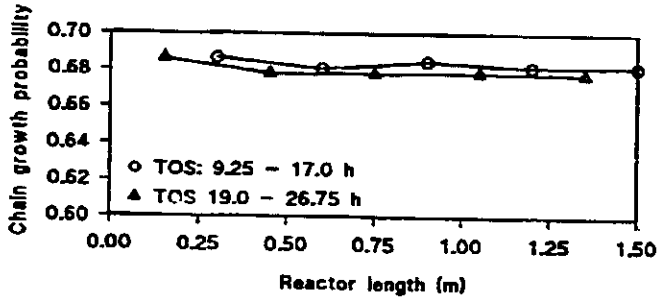

Run 3

Figure 5–4. Chain growth probability, α, dependent on axial reactor position and time on stream. The data points were recorded in sequence from inlet to outlet within the specified time intervals. Experimental conditions are given in table 5–1.

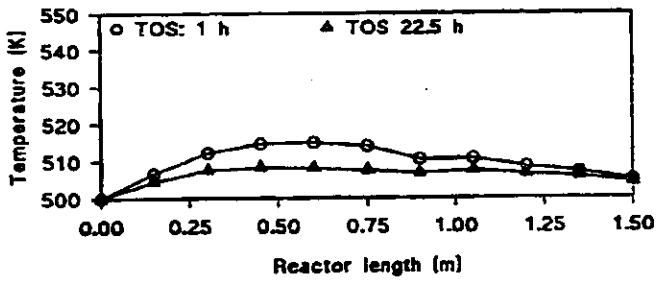

Run 1

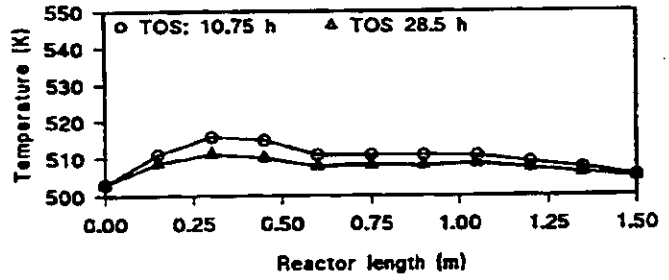

Run 2

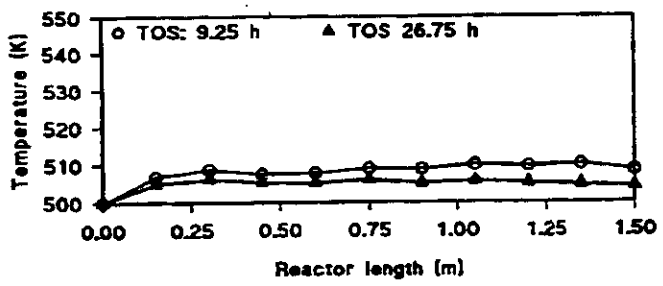

Run 3

Figure 5–5. Centerline temperature profiles recorded at different times. Experimental conditions are given in table 5–1.

5.3. KINETICS

5.3.1. Reactions and stoichiometry

The stoichiometry and heat of reaction for the synthesis of hydrocarbons are expressed by equation 5–1. For the synthesis of C_{2+} hydrocarbons the reaction enthalpy per mole CO converted is nearly independent of the carbon number while the heat of reaction for methane formation are somewhat higher as shown in equation 5–2. The temperature dependence of the reaction enthalpy is minor (Mc Ketta, 1985).

$$CO + (2+1/n)H_2 \rightarrow (1/n)C_nH_{2n+2} + H_2O, \quad \Delta H_R = -165 \text{ kJ} \qquad (5\text{–}1)$$

$$CO + 3H_2 \rightarrow CH_4 + H_2O, \quad \Delta H_R = -215 \text{ kJ} \qquad (5\text{–}2)$$

If CO_2 selectivity is of importance the water–gas shift reaction and possibly the Boudouard reaction must be taken into account, but these reactions are neglected in this study. It follows from chapter 5.2 that with a few exceptions the CO_2 selectivity is low. Furthermore, the CO_2 concentration analyses are not very accurate due to low concentrations and a bad base–line on the chromatograms in the CO_2 region. The points in the reactor where the analyses showed unusual high CO_2 selectivity were omitted in the parameter estimations. These were the concentrations measured at z = 1.35 m in run 2 and 3.

The modeling was concerned with the conversion of CO and the formation of CH_4 according to equations 5–1 and 5–2, necessitating only calculation of the concentration profiles of CO, H_2 and CH_4. The rate of H_2 consumption are in addition to the dependence on the rates of CO consumption and CH_4 formation, also dependent on the carbon number distribution of the C_{2+} fraction according to equation 5–1. This distribution was described by the Schulz–Flory parameter α for C_{3+} and the C_2/C_3 ratio γ for C_2. These parameters were considered constant, independent of reactor position and time, and the values were obtained from the analyses at the reactor outlet. The values obtained for the three runs are given in Appendix II and in Table 4–2.

The selectivity parameters are dependent on temperature (Lee and Anderson, 1984) and the partial pressures of CO and H_2, but since there are small variations in temperature and the CO/H_2 ratio, the variations are expected to be small. These assumptions are confirmed by the data in Appendix II and Figure 5–4.

5.3.2. Model and parameter selection

The relatively simple Langmuir–Hinshelwood type equation 2–46 proposed by Yates and Satterfield (Yates and Satterfield, 1991) was chosen as the basis for the calculation of the rate of CO consumption because it was shown to correlate well with experimental data from several investigations. The same relation was also recommended for the calculation of the rate of methane formation (Yates and Satterfield, 1992).

In equation 2–46 both the rate constant and the adsorption constant are dependent on temperature as shown in equation 2–51. It was not possible to quantify these dependencies from the experiments performed in this study because of the small variations in temperature. Therefore, the activation energy and adsorption enthalpy had to be evaluated from literature data.

A wide range of values has been reported for the activation energy of cobalt based Fischer–Tropsch catalysts, and the values varies with support, preparation and metal loading (Reuel and Bartholomew, 1984). For CO conversion on SiO_2 supported cobalt catalysts values between 32 and 131 kJ/mol have been reported (Reuel and Bartholomew, 1984), but most reports find values in the range 90 – 100 kJ/mol (Yates and Satterfield, 1991). There are fewer reports on values for the activation energy of methane formation, but the values are generally 20 – 60 kJ/mol higher than the values reported for CO consumption (Reuel and Bartholomew, 1984).

The observed activation energies using a homogeneous reactor model may also be lower than the actual ones if intraparticle mass transfer limitations are of importance (Satterfield, 1970). It is known that severe mass transport diffusional limitations may exist in the catalyst pores

if the pores are filled with liquid hydrocarbon products (Iglesia et al., 1993). This will make the apparent activation energy dependent on catalyst particle size. For a cobalt catalyst promoted with zirconium an approximate halving of the apparent activation energy for the rate of CO conversion was observed for catalyst particles of 2.4 mm diameter compared with 0.38 mm particles (Sie et al., 1991). The observed activation energy was 120 kJ/mol for the 0.38 mm particles and 60 – 70 kJ/mol for the 2.4 mm particles. It follows from the discussion in chapter 5.2 that it is not likely that the catalyst pores were completely liquid filled during the time that the measurements were performed for the experimental runs reported here. Thus, the degree of diffusional limitations were not known. If liquid accumulation in the pores occured during the time of the analyses, both a time and reactor positional dependency on activation energies can be expected.

Due to the uncertainties regarding the values of the activation energies of the catalyst used in this study and the unknown degree of intraparticle diffusional mass transfer resistance, two different sets of values for the activation energies are used in the simulations. One set is in the high range and the other in the low range of the values reported in the literature. The selected values are shown in Table 5–2.

The adsorption constant of CO depends on temperature according to equation 2–51. Very few reports are published on this temperature dependence for cobalt catalysts. Huff and Kobylinski (Huff and Kobylinski, 1991) have estimated a value of 25 kJ/mol for the adsorption enthalpy and 113 kJ/mol for the activation energy when fitting experimental kinetic data to a Langmuir–Hinshelwood expression similar to equation 2–46. Thus the temperature dependence of the rate constant seems much more pronounced than the temperature dependence of the adsorption constant. Because of this result and the lack of any estimate of the value of the adsorption enthalpy for CO for the catalyst used in this study, it was decided to neglect the temperature dependence of K_{CO} in the model.

Equation 2–46 was used in the preliminary kinetic evaluations, both for the modeling of the rate of CO consumption and the rate of methane formation. A time dependent activity term shown in equation 5–3 was included in the rate expression to account for the observed deactivation.

Initially a pseudo–homogeneous model including both heat and mass transport was applied in the attempt to estimate the kinetic parameters, i.e. the preexponential factors, the rates of deactivation and the adsorption constant. The model was of the traditional type with constant void fraction, velocity and dispersion coefficients across the bed.

In the first instance, the correlations recommended by Vortmeyer and Haidegger (Vortmeyer and Haidegger, 1991) shown in equations 2–21 to 2–24 were used in estimation of the axial and radial dispersion coefficients. However, this approach failed due to the use of a too low value for the effective radial thermal conductivity, predicted by equation 2–24. With this low value of the radial conductivity, heat transfer to the coolant could not be properly matched to the heat production, and the solution of the model equations was unable to converge to a steady state.

Then an estimation of both kinetic parameters and the effective radial conductivity was tried. The kinetic parameters and the radial conductivity were estimated by fitting the model output to the concentration and temperature data from the three steady state experiments, using a weighted least square criterion of fit. Due to expected differences in initial catalyst activity and rate of deactivation for the three experimental runs, the three runs were treated separately estimating a set of parameters for each run. However, the least square object function showed an evident lack of a distinct minimum, using this approach with the experimental data, thus making accurate parameter estimates impossible. The values of the estimated parameters were to a considerable extent dependent on the choice of initial values. Furthermore, the traditional dispersion model was not able to give a very good description of the observed temperature profiles as shown in chapter 5.4.3.

It was therefore decided to estimate kinetic parameters using a pseudo–homogeneous model for mass transport only, fitting the calculated concentration profiles to the experimental data and using the measured temperature profiles for the calculation of reaction rates. This decision was taken on the generally accepted basis that mass transport is more "plug–flow" in nature than heat transport. Most simulations under steady state conditions predicts nearly flat radial concentration profiles (Doraiswamy and Sharma, 1984, p. 228). This makes the mass transport model relatively insensitive to the values used for the dispersion coefficients and consequently

exact knowledge of their values is not necessary.

The orthogonal collocation method, used for radial discretization, sets constraints on the choice of radial positions where concentrations are calculated in the model. If the points do not coincide with the position of the thermocouples, interpolation between the measured temperatures has to be made. This, however, requires some knowledge or assumptions as for the shape of the radial profiles, especially when the profiles are steep or there are few radial measurement positions.

To avoid making such assumptions it was decided to use the mass balance equation 4–2 with one radial collocation point in kinetic parameter estimation and to use the temperature profiles measured at $r' = 0.577$ as a representation of the mean radial temperature. This approach is equivalent to the one–dimensional plug–flow model with axial dispersion and varying axial temperature. The axial dispersion coefficient was calculated from equation 4–9, and the rate constants were calculated from the temperature measurements at $r' = 0.577$.

Simultaneous estimations of preexponential factors and the inhibiting effect of CO expressed by the adsorption constant K_{CO} revealed strong correlation between the parameters, making accurate estimates difficult. With an initial choice for the value of K_{CO} in the range 14 – 20 1/MPa, the parameter estimation did not alter this value to any extent, but instead adjusted the activity and deactivation parameters to obtain the best fit, and the goodness of fit seemed fairly independent of K_{CO} within this range. Although estimated activity and deactivation parameters differed for the three experiments, the range of K_{CO} was the same. It was thus concluded that the value of K_{CO} was in the range of approximately 14 – 20 1/MPa which is in agreement with the values reported by Yates and Satterfield (Yates and Satterfield, 1991) of 11.61 1/MPa at 493 K and 22.26 1/MPa at 513 K for a Mg promoted cobalt on SiO_2 catalyst. From these findings if was decided to fix the value of K_{CO} at 17 1/MPa in the simulations and estimations of catalyst activity and deactivation rates for the three experimental runs.